



Amorphous polymer dynamics and free volume element size distributions from ultrafast IR spectroscopy

David J. Hoffman^a, Sebastian M. Fica-Contreras^a, and Michael D. Fayer^{a,1}

^aDepartment of Chemistry, Stanford University, Stanford, CA 94305

Contributed by Michael D. Fayer, April 17, 2020 (sent for review February 20, 2020; reviewed by Mischa Bonn, Aaron Massari, and Martin T. Zanni)

A method for measuring the size and size probability distribution of free volume regions in polymeric materials using ultrafast infrared (IR) polarization-selective pump-probe experiments is presented. Measurements of the ultrafast dynamics of a vibrational probe (the CN stretch of phenyl selenocyanate) in poly(methyl methacrylate) show that the probe dynamics are highly confined. The degree of confinement was found to be both time-dependent and dependent on the vibrational frequency of the probe molecule. The experiments demonstrate that different vibrational frequencies correspond to distinct subensembles of probe molecules that have different dynamic properties determined by their local structural environments. By combining the degree of dynamical confinement with the molecular size of the probe molecule, the free volume element size probability distribution was determined and found to be in good agreement with the best established experimental measure of free volume. The relative probability of a free volume element size is determined by the amplitude of the nitrile absorption spectrum at the frequency of the measurement. The inhomogeneous broadening of the spectrum was linked to the vibrational Stark effect, which permits site selectivity. The observed dynamics at each frequency were then associated with a different size free volume element and distinct local electric field. The multiple timescales observed in the pump-probe experiments were connected to local structural fluctuations of the free volume elements.

polymers | dynamics | ultrafast IR spectroscopy | free volume | Stark effect

The concept of free volume in polymers (1)—void spaces that arise from the inefficient packing of polymers due to their long-chain amorphous nature—is fundamental to nearly every aspect of polymer behavior. Free volume directly determines transport properties (2, 3) and aging effects (4–6) and can be associated with mechanical deformation (7, 8), thermal expansion (9), and electrical strength (10). Despite the theoretical significance of free volume, only a handful of techniques can estimate the average size of the actual free volume elements (FVEs) in a polymer, and even fewer techniques can provide a measure of the distribution of FVE sizes (4, 11, 12). This is due to the extremely small dimensions of FVEs (only a few angstroms in radius) and their structurally transient nature.

This paper describes the restricted orientation anisotropy method (ROAM) for studying structural dynamics of polymeric materials and measuring the distribution of FVE sizes using ultrafast infrared (IR) polarization-selective pump-probe spectroscopy (PSPP). In particular, PSPP experiments were used to measure the orientational relaxation (13–17) of the small long-lived vibrational probe phenyl selenocyanate (PhSeCN) in the amorphous polar polymer poly(methyl methacrylate) (PMMA). The orientational relaxation is shown to be highly restricted, indicating that the probe molecules are limited in their motion due to the confinement of the polymer surroundings. By combining the degree of orientational confinement experienced by the probe with the molecular dimensions of the probe molecule,

the sizes of the void spaces experienced by the probe molecules were obtained.

It was found that the degree of orientational confinement measured by the PSPP experiments depended strongly on the vibrational frequency within the inhomogeneously broadened spectrum of the PhSeCN probe molecule's CN stretch. The observed frequency dependence was associated with distinct structural environments for PhSeCN in the PMMA matrix. The frequency dependence of the restricted orientational relaxation across the inhomogeneously broadened spectrum is caused by differing degrees of spatial confinement experienced by PhSeCN in PMMA. Relating the frequency dependence of the spatial confinement to the vibrational frequency distribution (spectrum) yields the probability distribution of FVE sizes in the polymer.

In a polymeric solid, the size and the range of angles sampled by a probe molecule make it possible to determine the radius of the FVE at each frequency across the vibrational absorption spectrum. Unlike previous methods for determining the free volume distribution, the PSPP measurements also provide information on the dynamical evolution of the FVEs. In the picosecond-to-nanosecond time regime over which the pump-probe experiment can measure the orientational dynamics of the PhSeCN probe molecule, three separate timescales of confinement are identifiable: one that occurs on subpicosecond time-scale (inertial relaxation) and is only weakly frequency-dependent and two that occur on 10-ps and 200-ps timescales that have strong frequency dependences. The angular range sampled on 200-ps timescales was associated with the free

Significance

The free volume content of polymers has immense importance for polymer properties. However, it is extremely difficult to measure the properties of the free volume elements (FVEs) that make up the free volume. Here we employ ultrafast infrared (IR) pump-probe spectroscopy to measure the properties of the nanoscopic FVEs in polymers using small-molecule IR probes. With this new method, the size and size distribution of the FVEs in polymers are measured and found to agree with previous measurements. The IR measurements also show that the FVEs undergo ultrafast structural fluctuations and provide a way to measure the distribution of local electric fields in the FVEs, which are correlated with the size of the FVEs.

Author contributions: D.J.H. and M.D.F. designed research; D.J.H. and S.M.F.-C. performed research; S.M.F.-C. contributed new reagents/analytic tools; D.J.H. and M.D.F. analyzed data; and D.J.H., S.M.F.-C., and M.D.F. wrote the paper.

Reviewers: M.B., Max Planck Institute for Polymer Research; A.M., University of Minnesota; and M.T.Z., University of Wisconsin–Madison.

The authors declare no competing interest.

Published under the [PNAS license](#).

¹To whom correspondence may be addressed. Email: fayer@stanford.edu.

This article contains supporting information online at <https://www.pnas.org/lookup/suppl/doi:10.1073/pnas.2003225117/-DCSupplemental>.

volume available averaged over the structural motions in the polymer, and the range sampled on the 10-ps timescale was determined to be representative of the instantaneous free volume distribution present in the polymer. It also indicates that the FVEs in PMMA undergo a degree of structural evolution on the timescale of tens of picoseconds.

The frequency dependence of the PhSeCN nitrile stretch was associated with the first-order vibrational Stark effect. The magnitude of the Stark effect was determined by examining the vibrational solvatochromism of PhSeCN in common solvents and comparing the magnitude of the shift to benzonitrile, for which both the solvatochromism and explicit Stark coupling parameters have been determined (18). The calculated local electric fields are not large enough to create the observed restricted orientational relaxation, which is therefore assigned to steric confinement by the polymer matrix FVEs. However, the field strengths were found to be large enough to cause the probe molecules to have some tendency to align with the local electric field. By describing the frequency shift with a vibrational Stark effect, the frequency-dependent orientational confinement experienced by the PhSeCN probes was assigned to both an FVE size and a local electric field.

The size distribution measured by the PSPP experiments was comparable to those reported for PMMA using positron annihilation lifetime spectroscopy (PALS) (19). The PSPP-measured short time distribution was found to be in very good agreement with PALS results, which is the best-established technique for measuring FVEs. This demonstrates the appropriateness of the assumptions made in calculating the FVE radius using the probe orientational relaxation data.

Experimental Procedures

Sample Preparation.

PMMA films. PMMA (molecular weight [Mw] 350,000) and PhSeCN were purchased from Sigma-Aldrich and used as received. A PMMA polymer film with dissolved PhSeCN was solvent-cast from chloroform. Briefly, the density of PMMA was used to determine the mass of polymer needed to create a 3- × 3-in. film, 250 μm in thickness. PMMA was dissolved in excess chloroform (~20 mL) and an appropriate volume of PhSeCN was added to the solution to be 2.5 mol % with respect to the PMMA monomer unit. The resulting solution was sonicated and deposited on a large glass plate, leveled by a micrometer-controlled stage, and the chloroform was allowed to evaporate overnight. The solution was kept in place by a 3- × 3-in. four-sided open glass cube attached to the glass plate, and it was observed that a large volume of chloroform facilitated the formation of a film with uniform thickness. Partially covering the top of the box to slow down the evaporation of chloroform prevented the formation of bubbles and increased the optical quality of the sample. Once chloroform evaporated, a structurally sound film of excellent optical quality was peeled off the surface of the glass. A 20-mm-diameter disk was cut out and dried under vacuum (<100 mtorr) at 90 °C for 4 d to remove the remaining solvent from the film. The resulting dry film was moved to a glove box, where it was sandwiched between two CaF₂ windows and assembled into a sealed copper cell to hold the sample in position during experimental measurements.

Low-Mw PMMA samples. The low-Mw PMMA oligomer (Mw 500, polydispersity 1.19) was purchased from Agilent Technologies and used as received. Approximately a gram of PMMA (a viscous fluid) was removed from the vial and weighed. PhSeCN was added to the vial by micropipette to reach 3 mol % concentration relative to the PMMA monomer units. The solution was gently heated and sonicated for about 6 h to allow them to mix. The solution was then deposited onto a CaF₂ window and sandwiched between a second CaF₂ window separated by a 150-μm Teflon spacer. The two windows were placed in a sealed copper sample cell to produce good thermal contact. The copper sample cell was placed so that the windows were vertical and then heated gently to allow the material to flow and make good contact with both windows. For temperature-dependent IR experiments, the sample cell was attached to a Peltier thermoelectric cooler that could maintain temperature stability to ±0.1 K.

PhSeCN solvent standards for Fourier transform IR experiments. Ten molecular solvents (Acros: dimethyl sulfoxide and tetrahydrofuran; Sigma-Aldrich: carbon tetrachloride and methyl acetate; Millipore: dichloromethane; Fisher Scientific: all others) were used as acquired. Solutions of each were prepared with 3 mol % PhSeCN. Drops of each solution were placed on a CaF₂ window

and sandwiched between a second CaF₂ window with a 150-μm Teflon spacer and secured in a sealed copper sample cell.

Fourier Transform IR Measurements. Fourier transform IR (FTIR) measurements were performed on a Nicolet 6700 FTIR spectrometer (Thermo-Fisher Scientific) at 1-cm⁻¹ resolution. As PMMA and many of the molecular solvents have background absorption in the region of the PhSeCN nitrile absorption (2,130 to 2,170 cm⁻¹), background subtraction was performed using a spectrum without the PhSeCN molecule. Optical densities of the nitrile mode ranged from 0.2 to 0.4, which is the ideal range for nonlinear IR experiments.

Ultrafast IR equipment. Descriptions of analogous laser systems and experimental techniques can be found in previous publications (20, 21). Briefly, a commercial Ti:Sapphire (Spitfire ACE; Spectra-Physics) regenerative amplifier produces a 2-mJ pulse of 800-nm light at a 3-kHz repetition rate. The 800-nm light pumped a home-built optical parametric amplifier to convert the 800-nm light to mid-IR light at 4.6 μm, resonant with the PhSeCN nitrile stretch. The mid-IR pulse energy is 30 μJ at a 3-kHz repetition rate. The pulses have 100-cm⁻¹ bandwidth and are near transform-limited.

For the PSPP experiments, the mid-IR pulse is split into a strong pump (~90% intensity) and weak probe (~5% intensity) pulse. The pump pulse goes through a germanium acousto-optical modulator (AOM) which functions as a pulse shaper. The probe pulse goes down a mechanical delay stage to provide a variable time delay of nearly 2 ns. The pump and probe pulses are then overlapped in the polymer sample. The pump pulse's polarization is rotated with a half-wave plate to +45° relative to the probe pulse and passed through a polarizer at +45° prior to the sample. The probe pulse is then polarization resolved after the sample at +45° (parallel) and -45° (perpendicular) and frequency-resolved using a monochromator with a 32-pixel mercury cadmium telluride array detector. The AOM then functions to block every other pump shot, and the transient absorption signal is measured as the difference in intensity in the probe between the shots with the pump "on" and the pump "off." This process is repeated for a wide range of time delays and in both the parallel and perpendicular polarizations.

IR Spectroscopy of the Polymer Films

PSPP. The pump-probe experiment can be understood qualitatively as follows. First, a strong "pump" pulse of IR light excites an anisotropic subset of the PhSeCN probe molecules that have their nitrile bond aligned preferentially with the direction of the polarization of light. The frequency of the IR light is tuned to be resonant with the nitrile stretch of PhSeCN as determined by FTIR spectroscopy. The FTIR spectrum is shown in Fig. 1A. Excitation to the vibrational excited state does not perturb the sample. After excitation, the probe molecules can undergo angular diffusion, which gradually causes them to become more isotropically (randomly) oriented. At a time t later, a second "probe" pulse passes through the pumped region of the sample with either the same or orthogonal polarization as the pump pulse. The probe pulse experiences a bleach of the ground vibrational state and stimulated emission from the first excited state in the frequency region of the vibrational absorption (0-to-1 transition) as well as an excited vibrational state absorption in the frequency range of the 1-to-2 transition. The 1-to-2 transition is shifted to lower frequency by the vibrational anharmonicity (Fig. 1B). The intensities of parallel and perpendicular polarization signals depend on the square of the projection of the PhSeCNs' transition dipoles on the polarization of the probe pulse. If the initial cosine squared distribution excited by the pump, which is aligned along the parallel direction, has changed little, the parallel signal's intensity will be much higher than the perpendicular signal's intensity. If instead the distribution is isotropic (the transition dipole directions have randomized), then the signals for the two polarization will have the same magnitude. By varying the time t between pump and probe and tracking the change of the difference between the parallel signal intensity (I_{\parallel}) and the perpendicular signal intensity (I_{\perp}), the rate of orientational relaxation can then be quantified.

The time-dependent intensities of these signals are given by (13, 14)

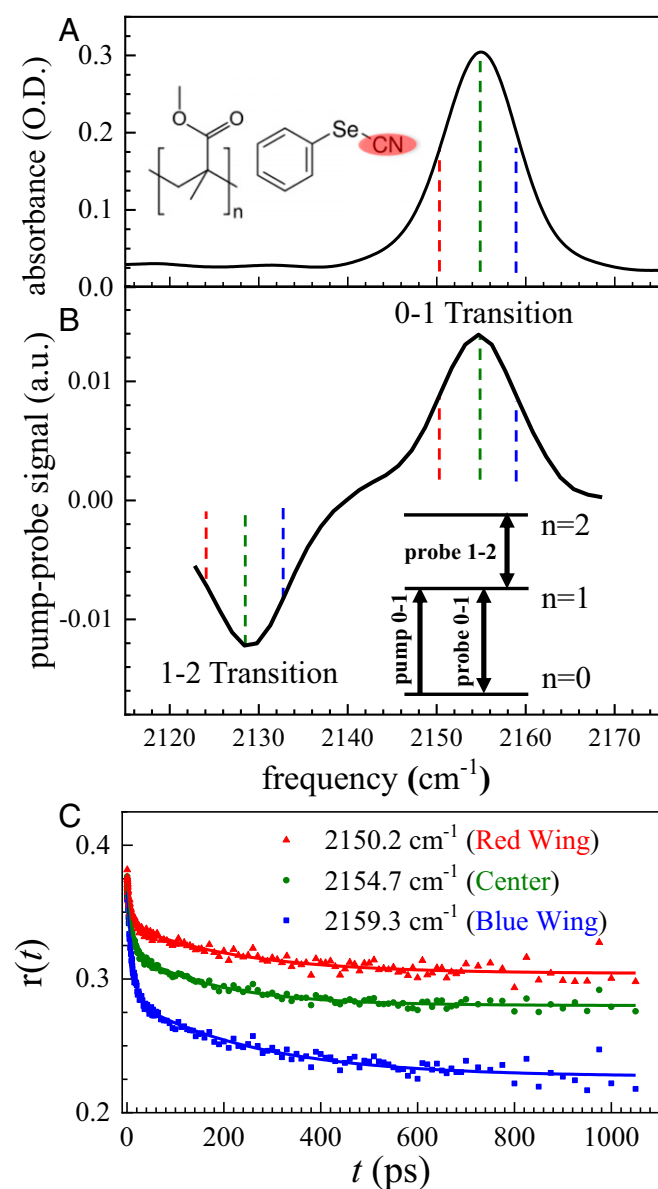


Fig. 1. Spectra and pump-probe data of PhSeCN in PMMA. (A) FTIR spectrum of the CN stretch of PhSeCN in PMMA. (Inset) Chemical structures of PhSeCN and PMMA. (B) A transient absorption spectrum measured by the pump-probe experiment on the CN stretch of PhSeCN in PMMA. The ground state 0-to-1 and excited state 1-to-2 transitions are shown. (Inset) Vibrational energy level diagram for the pump-probe experiment indicating the two transitions. (C) Pump-probe anisotropy decays (orientational relaxation) for representative vibrational frequencies of PhSeCN in PMMA. The orientational dynamics are restricted to a limited range of angles and highly frequency-dependent. Solid lines are fits to Eq. 4.

$$\begin{aligned} I_{\parallel} &= P(t) \left(1 + \frac{4}{5} C_2(t) \right) \\ I_{\perp} &= P(t) \left(1 - \frac{2}{5} C_2(t) \right). \end{aligned} \quad [1]$$

$P(t)$ is the isotropic signal, which is the vibrational population lifetime of the first excited state of the CN stretch of PhSeCN. $C_2(t)$ is the second Legendre polynomial orientational correlation function, which describes the rate of orientational relaxation of the probe molecules. $C_2(t)$ is given by

$$C_2(t) = \langle P_2(\cos \gamma) \rangle, \quad \cos \gamma = (\hat{\mu}(t) \cdot \hat{\mu}(0)), \quad [2]$$

where $\mu(t)$ is the orientation of the transition dipole at time t (which for the measured CN stretch of PhSeCN is essentially along the permanent CN bond), P_2 is the second Legendre polynomial, and $\langle \dots \rangle$ denotes an ensemble average. $P(t)$ and $C_2(t)$ can then be determined from the signal intensities in Eq. 1:

$$\begin{aligned} P(t) &= (I_{\parallel} + 2I_{\perp})/3 \\ r(t) &= \left(\frac{I_{\parallel} - I_{\perp}}{I_{\parallel} + 2I_{\perp}} \right) = 0.4C_2(t), \end{aligned} \quad [3]$$

where $r(t)$ is called the anisotropy.

The isotropic signal, $P(t)$, shows that the vibrational population of the PhSeCN decays exponentially with a lifetime of 446 ± 8 ps across the entire absorption band. This lifetime is very similar to the lifetime of PhSeCN measured in other non-H-bonding chemical systems (22). The vibrational lifetime determines the maximum timescale that is measurable in the pump-probe experiment: Typically, signals out to several factors of the lifetime are measurable. The isotropic signal additionally reveals that there is a heating signal in the pump-probe spectra at long waiting times, which was corrected for to extract the orientational dynamics of the probe. Details on eliminating the heating effects can be found in *SI Appendix*.

Orientalional Dynamics. In contrast to the relatively simple behavior of the population dynamics, the anisotropic orientational dynamics display both strongly nonexponential behavior and have a strong systematic vibrational frequency dependence. The pump-probe anisotropies for representative frequencies of the absorption spectrum are plotted in Fig. 1C. A biexponential decay to an offset describes the anisotropies at all frequencies (solid curves in Fig. 1C). This encompasses a fast decay that occurs on a ~ 10 -ps timescale and a slower decay on a ~ 200 -ps timescale. The decays go to the offset (a plateau) at long times (~ 1 ns). The plateau is the result of a persistent probe molecule orientational anisotropy on a timescale long compared to the experiments. That is, the probe molecules cannot undergo complete orientational randomization on a timescale of nanoseconds. Finally, there are deviations from perfect correlation of 0.4 at short time, which is caused by ballistic (inertial) orientational motions that occur on timescales faster than the experiment can resolve (23).

To describe the biexponential decays to an offset that were measured in the PhSeCN/PMMA system, the following parameterization was employed (24):

$$C_2(t) = S_0^2(S_1^2 + (1 - S_1^2)\exp(-t/\tau_1))(S_2^2 + (1 - S_2^2)\exp(-t/\tau_2)), \quad [4]$$

where S_0 , S_1 , and S_2 are order parameters that account for the extent of restricted angular motion during the inertial process, the first diffusive process, and the second diffusive process, respectively. The order parameters can be associated in a model-independent manner with a characteristic angle, γ_i , through Eq. 2 (25), which is $\sqrt{\langle \gamma^2 \rangle}$ in the small-angle approximation. It will be useful to also consider the cumulative order parameters: These are simply $S_{0+1} = S_0S_1$ for the combined inertial and first diffusive order parameter and $S_{\text{tot}} = S_0S_1S_2$ for the total order parameter.

To describe the restricted orientational motion, the wobbling-in-a-cone model of orientational dynamics was used (Fig. 24) (24–27). In the model, the ensemble of PhSeCN probe molecules is free to reorient only within a certain range of angles which make up a cone. The cone in this case is determined by the structure of the surrounding polymeric matrix. Over a characteristic time, there is a

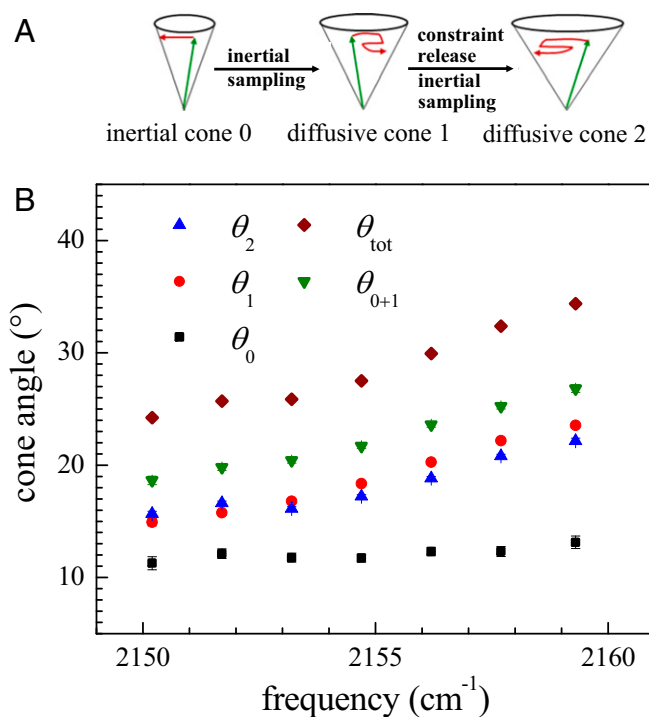


Fig. 2. The wobbling-in-a-cone model and results. (A) Schematic figure of the wobbling-in-the-cone model. The probe molecule can diffuse in a limited angular range defined by a cone angle θ_i until structural motions allow it to sample a larger angular volume. (B) Cone angles determined from fits of the frequency-dependent anisotropy using Eqs. 4 and 5. θ_{0+1} and θ_{tot} are cumulative cone angles, and θ_0 , θ_1 , and θ_2 are individual cone angles. The cone angles are highly frequency-dependent, reflecting the frequency dependence of the anisotropies.

partial constraint release caused by the dynamic motion of the polymer matrix, for example side groups, which enables further orientational relaxation within a new, larger cone. A cone half-angle θ_i from the wobbling-in-a-cone model is related to an order parameter, S_i , as follows:

$$S_i = \frac{1}{2} \cos(\theta_i)(1 + \cos(\theta_i)). \quad [5]$$

The cone half-angle reflects the maximum extent of angular motion in the model for the i^{th} cone, which can be shown to be $\sim 1.5\gamma_i$. The fit parameters using Eqs. 4 and 5 for the entire range of 0-to-1 transition frequencies can be found in *SI Appendix*, Table S1. The individual and cumulative cone angles are plotted in Fig. 2B. An identical trend between the cone angles and vibrational frequency can also be found using data from the 1-to-2 transition (*SI Appendix*).

It is striking that in the PhSeCN/PMMA data the pump-probe anisotropy decays are highly frequency-dependent (Fig. 1C). The angles of the diffusive cones θ_1 and θ_2 also change substantially and continuously across the CN absorption band (Fig. 2B). In general, this contrasts with observations of orientational relaxation of vibrational chromophores in other types of systems. To the authors' knowledge, frequency-dependent orientational order parameters have only been seen previously for hydrogen-bonding systems, where the strength of a system's hydrogen bond interactions can determine both the frequency of the vibrational transition and the orientational mobility of the vibrational probe (23, 27).

In the wobbling-in-a-cone model, the frequency dependence demonstrates that different subensembles of PhSeCN molecules

experience distinct steric cones and orientational dynamics depending on their vibrational frequency. Both the frequency and the cone angles of a vibrational probe depend on its solvation environment (18). The distribution of cone angles then maps to a distribution of probe frequencies measured by FTIR. This distribution of confinement is conceptually similar to the distribution of FVE sizes that exist in amorphous polymers (4, 12, 28). θ_0 is virtually frequency-independent (Fig. 2B). It reflects single steps in the angular walks that sample the FVEs. As discussed in detail below, the range of angles sampled depends on the sizes of the FVEs, and the sizes are correlated with the frequency. So, θ_1 and θ_2 , which result from complete angular sampling of FVEs, vary with size and therefore frequency, while θ_0 is independent of frequency. A method for connecting the cone angles to the FVE sizes will be developed in *Calculating FVE Size and Size Distribution from Cone Angles*.

Suppressing the frequency dependence in low-Mw PMMA. For the frequency-dependent anisotropy decays to occur, the transition frequencies of probe molecules must be essentially constant over the experimental timescale. If the frequencies of the vibrational probes were able to randomize within the inhomogeneous spectrum on a timescale short or comparable to the experiment, then a probe's dynamics would not be associated with a well-defined frequency (structural environment). This correlation can be examined quantitatively with two-dimensional (2D) IR spectroscopy. For a glassy solid like PMMA, it has been previously shown that the transition frequency remains highly correlated on these timescales (29), and 2D IR experiments on the PhSeCN in PMMA system confirm this picture (*SI Appendix*).

Previous 2D IR experiments on small-molecule glass-forming liquids show that the dynamics that randomize the vibrational frequency can often be associated with the viscosity of a liquid system (22). Raising the temperature of a glass former well above the glass transition then leads to rapid decorrelation. Heating the high-Mw PMMA/probe system to the point where it would become sufficiently liquid-like to observe fast decorrelation (and presumably loss of frequency-dependent orientational relaxation) would cause the PhSeCN probe molecules to either volatilize or decompose.

It has been well established that as the Mw of a polymer becomes lower, the glass transition temperature becomes lower and the polymer becomes more liquid-like (30, 31). Therefore, in a sufficiently low-Mw PMMA sample, that is, an oligomer, the frequency dependence of the reorientation should turn off once the viscosity becomes low enough to permit complete frequency decorrelation on sufficiently fast timescale. Comparing a low-Mw PMMA sample to the high-Mw PMMA sample described above also keeps the intermolecular interactions as similar as possible, as the only difference is in the chain lengths and the density of the polymer end groups.

Toward this end, a very-low-Mw PMMA oligomer sample (500 atomic mass units, corresponding to only approximately five repeat units on average) was prepared with PhSeCN. FTIR spectroscopy confirms that the PhSeCN experiences a similar environment in the low-Mw PMMA: The absorption in the low-Mw PMMA is centered at $2,155.2 \text{ cm}^{-1}$ with a full width at half maximum (FWHM) of 10.2 cm^{-1} , while it is at $2,154.9 \text{ cm}^{-1}$ and 10.4 cm^{-1} in the high-Mw PMMA (spectra in *SI Appendix*). Pump-probe decays and 2D IR spectra were taken of the low-Mw PMMA sample at two temperatures: 260 K, close to its glass transition temperature of 244 K (31), and 360 K, well into the liquid regime. The 2D IR experiments on this chemical system showed the desired slow decorrelation at low temperatures and fast decorrelation at high temperatures (*SI Appendix*).

The frequency-dependent pump-probe anisotropies at these two temperatures are presented in Fig. 3. At low temperature, a frequency dependence in the pump-probe anisotropy, similar to that in the high-Mw polymer, was observed. However, once the

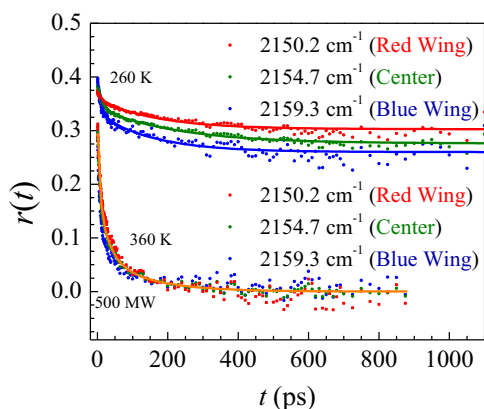


Fig. 3. Frequency-dependent pump-probe anisotropies for a low-Mw PMMA oligomer at high (360 K) and low (260 K) temperatures. The low-temperature data have frequency dependence resembling the high-Mw PMMA data, but at high temperature the frequency dependence is greatly suppressed.

low-Mw PMMA oligomer was heated far above the glass transition temperature, the frequency dependence can be seen to be greatly reduced, with the differences almost within experimental error. The remaining frequency dependence is only substantial at short times where the transition frequency correlation is still significant. The frequency/orientational relaxation correlation can be observed and then suppressed in a single system by increasing the temperature well above T_g .

Calculating FVE Size and Size Distribution from Cone Angles

The Probe Molecule as a Molecular Ruler. The size of the confining volumes for PhSeCN can be determined using a model that couples the range of angles sampled by the probe in a wobbling-in-a-cone model, the molecular dimensions of PhSeCN, and the FVE radii. The ROAM model works as follows. We consider rotating the PhSeCN molecule around an axis perpendicular to the transition dipole that goes through the center of mass of the molecule. The cone angle corresponds to the magnitude of rotation on that axis (Fig. 4A). The radius r_i of the volume element swept out by a given cone is then $r_i = a \sin \theta_i + \Delta r$, where θ_i is the cone angle from the wobbling-in-a-cone analysis, a is a molecular distance from the center of mass, and Δr is an effective van der Waals radius of a molecular moiety that contacts the surface of the FVE. The measurable range of FVE radii based on this model then goes from Δr to $a + \Delta r$. By applying this metric to the frequency-dependent cone angles, the frequency-dependent FVE radii are determined. The measured FVE radius will correspond to the average FVE radius experienced by the subensemble of probes at a given frequency. This allows the vibrational frequency distribution to be directly related to an FVE radius probability distribution.

As it is necessary to select the dimensions a and Δr for PhSeCN, two limiting cases were examined. The lower limit considers only the van der Waals radius of the atom furthest from the center of mass, which was determined from a density functional theory (DFT) calculation (*SI Appendix*) to be the hydrogen atom in the *para* position to the SeCN. The values for the *p*-hydrogen case are $a = 4.3 \text{ \AA}$ and $\Delta r = 1.2 \text{ \AA}$ (32). The larger limit approximates the entire phenyl ring as a sphere and again uses distances from the DFT calculation and the van der Waals radii of the relevant atoms (32). The radius of the sphere was chosen to be the average of the widest (3.4 \AA) and narrowest (1.7 \AA) dimensions of the phenyl ring, giving values for the phenyl ring case of $a = 2.0 \text{ \AA}$ and $\Delta r = 2.5 \text{ \AA}$.

The results for the *p*-hydrogen and phenyl ring models are shown as cumulative distribution functions (CDFs) in Fig. 4 B

and C, respectively. The CDFs are acquired by taking the FVE radius at each frequency, multiplying it by the spectral amplitude of the area normalized absorption spectrum (Fig. 1A), and integrating to the particular CDF value. The black points are obtained from the first diffusive cone (θ_{0+1}). The timescale of this data is 10 ps. This timescale is fast compared to local polymer structure fluctuations, which occur on the several hundred picosecond timescale, and produces the second diffusive cone (θ_2). The second diffusive cones (θ_2) combine with the θ_{0+1} to yield the total cone angles, θ_{tot} . The total cone angles give rise to a dynamical measure of the FVEs, which are shown as the red points in Fig. 4 B and C. The relationship between the total cone angles and the FVE dynamics will be described following the discussion of the FVE radii determined from the first diffusive cone (black points) and comparison to measurements from the literature made with PALS, the blue curves in Fig. 4 B and C labeled PALS.

The *p*-hydrogen model results in smaller radii and a broader distribution than the phenyl ring model. However, the difference in the radii, r_{0+1} , in the middle of the two distributions (CDF = 0.5) is only 0.3 \AA . This shows that the ROAM method is robust as it is only mildly dependent on the very different choice of the contact moiety. Future experiments will use probes with different shapes, which will aid in determining how to parameterize the probe. It is important to emphasize that the pump-probe experiments directly measure the range of angles sampled by a

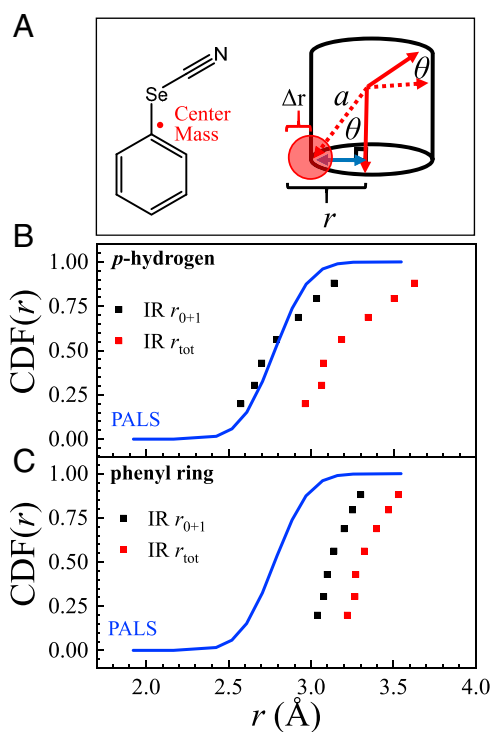


Fig. 4. The ROAM model and results for measuring the size of polymer FVEs. (A) The cylindrical volume element traced out by the PhSeCN molecule for a given cone angle θ . (B) Comparison of the CDFs of FVE radii r_{0+1} (black squares) and FVE shape fluctuations r_{tot} (red squares) from PhSeCN in PMMA using the *p*-hydrogen ROAM model (this work) and the literature free volume radii cumulative distribution measured by the PALS (19). The r_{0+1} distribution, which is the instantaneous FVE distribution, is very similar to the PALS distribution. (C) Comparison of the CDF of FVE radii r_{0+1} (black squares) and shape fluctuations r_{tot} (red squares) for the phenyl ring ROAM model CDFs to the PALS CDF. The r_{0+1} distribution, which is the instantaneous FVE distribution, is $\sim 0.3 \text{ \AA}$ larger than the PALS distribution.

vibrational probe. The issue is how to choose the appropriate probe dimensions to convert the measured cone angles into radii.

Comparison to PALS Measurements of the FVE Size Distribution.

Several techniques have been employed to measure FVE size distributions, or at least the average FVE size, of polymeric systems. The distribution of FVEs for PMMA has been measured with PALS (19, 33–35), which is the best established method for measuring FVE dimensions. Other methods that have been used to estimate FVE sizes in PMMA, the photoisomerization method (28, 36) and small-angle X-ray scattering (34), are discussed in *SI Appendix*.

PALS works by bombarding the polymer with positrons. PALS determines FVE sizes by measuring the rate of decay of the fraction of positrons that form metastable ortho-positronium (the triplet state) (12, 37, 38). The lifetime (~ 1 ns) of the metastable positronium can be related to the size of the FVE in which it is located. The FVE is taken to be a time-independent sphere with a radius, r , with a particular surface electron density. The quantum mechanical wave function for the positronium atom gives the positron spatial probability distribution. A more confined positronium atom (smaller FVE) has a shorter lifetime because of increased overlap between the positron's wavefunction and the electrons on the sphere surface. Complex numerical techniques convert the measured signal decay into a distribution of radii. Due to the small size of the positronium species (~ 1 Å) and the wide applicability of the technique, it is the most common method of measuring FVE distributions of polymers.

For PMMA at room temperature, the modal radius of the FVE measured by PALS in a number of studies is 2.7 to 2.8 Å (19, 33–35). The distribution of radii has only been explicitly reported in one publication, which are the blue curves shown in Fig. 4 *B* and *C* (19). As can be seen in Fig. 4*B*, the *p*-hydrogen model CDF and the PALS CDF are virtually the same. For the phenyl ring model (Fig. 4*C*), ROAM radii are somewhat larger than the PALS measurement. The ROAM *p*-hydrogen model also yields a modal radius of 2.8 Å, while the phenyl ring model gives a modal radius of 3.1 Å. The good agreement between the two experimental methods occurs despite the vast differences between PALS and ROAM in the methods of measurement and calculation of the sizes and distributions of FVEs. For instance, the PALS model assumes a time-independent FVE shape. Structural fluctuations, which occur on the hundreds of picosecond timescale in PMMA (Fig. 1*C*), that may facilitate or inhibit annihilation are not included in the model nor are they in the observable.

ROAM can reveal more than other methods because it provides dynamical information, for example FVE shape fluctuations (discussed below) not obtainable from other methods. In addition, a variety of vibrational probes can be employed. Different probes with different sizes and chemical behavior can each report on a complete free volume distribution if they satisfy two requirements. First, a probe must display sufficient solvatochromism so that different polymer microstructures yield distinct vibrational frequencies. However, even if a probe does not display different frequencies for different local polymer structures, the average FVE size can still be determined from the frequency-independent anisotropy decay. Second, a probe must have long enough vibrational lifetime to characterize the size of the first diffusive cone, θ_{0+1} . Intelligent probe selection can enable expanded experimental measurements of the sizes, shapes, dynamical, chemical, and electrostatic behavior of FVEs in polymers.

The Multiple Timescales and FVE Shape Fluctuations. Applying Eqs. 4 and 5 to the measured anisotropies yield a total of three cone angles. These cone angles and important combinations of them are shown in Fig. 2*B* as a function of frequency. θ_0 reflects the inertial steps taken on the ultrashort timescale. These steps can be thought of as the steps in a random walk. This random walk,

that is, diffusion, samples the first diffusive cone, which has an angular range (cone angle) of θ_{0+1} (green triangles in Fig. 2*B*). The first diffusive cone, which characterizes probe orientational motion on a ~ 10 -ps timescale, is strongly frequency-dependent and corresponds to a range of radii from 2.6 to 3.2 Å for the *p*-hydrogen model and 3.0 to 3.3 Å for the phenyl ring model (Fig. 4 *B* and *C* respectively, black squares). This range is sampled prior to the multicone model “constraint release” and is the measure of the sizes of FVEs in the polymer on a timescale short compared to significant polymer motions. The r_{0+1} is a measurement of the “instantaneous” FVEs of the polymer system.

The second diffusive cone, which contributes to the total sampled angular range θ_{tot} , follows significant constraint release from polymer structural rearrangements on a >10 -ps timescale. The additional angular range freed by the constraint release is virtually identical to that which is sampled by the first diffusive cone, that is, $\theta_1 \approx \theta_2$ for all frequencies (Fig. 2*B*). Therefore, for each subensemble with a given frequency, the spatial regions that give rise to FVEs are structurally fluctuating while on average conserving their total volume. In a particular FVE, some spatial regions become occluded by matter moving in while other spatial regions have matter moving out. The larger cumulative cone angles at longer time, θ_{tot} , are caused by the probes sampling angles that were blocked at short time.

The total cone angles, θ_{tot} , can then be related to larger radii. Applying ROAM to the total cone angle θ_{tot} gives radii of the FVEs for the total volume sampled from 3.0 to 3.6 Å for the *p*-hydrogen model and 3.2 to 3.5 Å for the phenyl ring model (red squares in Fig. 4 *B* and *C*, respectively). The increased radii reflect the total volumes accessible to the probe, but all of the accessible volume is not simultaneously accessible. If the volume had actually increased over hundreds of picoseconds, then θ_2 would be substantially greater than θ_1 , which is contrary to the data shown in Fig. 2*B*. As even hundreds of picoseconds is orders of magnitude faster than the structural dynamics of PMMA measured by techniques such as broadband dielectric spectroscopy (39, 40), the specific motions that cause the FVE shape fluctuations must be the result of the dynamics of small moieties, for example side groups or very small chain segments.

To appreciate the implications of the volume reflected by the total cone angle, consider the following analogy. A random walker is in a many-sided room of a certain area. He takes many random steps. When he hits a wall, he continues the random walk in another direction. After taking enough steps, he will have sampled the entire area of the room. A plot of all of his positions fills the room. If there are many walkers in many rooms with a wide variety of shapes but with a narrow distribution of areas around the average area, then a plot of all of the walker positions will look something like a filled circle with the average area. This is the equivalent to the first cone with the area corresponding to the angle θ_{0+1} .

The walkers keep walking. After a long time, the walls of the rooms move. Some of the walls move in toward the center and some of them move out, but the rooms' areas stay the same on average. The walkers are blocked from some regions they could access before but new regions are opened up, which are sampled. When the ensemble average of the positions of all of the walks in the long time walks (changed rooms) are plotted, they will look like a circle with the same area as the original set of short time walks (original rooms). This is the equivalent of $\theta_1 = \theta_2$. However, if all of the positions from the walks over the entire time range are plotted together, the total area will be larger, which corresponds to θ_{tot} . The moving walls (long time local polymer structural fluctuations) blocked some regions and opened up other regions, but the ensemble average area of the rooms did not change. However, the total area accessed increased. This combined short and long time sampling is the equivalent of the

red points in Fig. 4 B and C. The increased radii reflect shape fluctuations of the FVEs rather than increased FVE volumes.

The ROAM model can also be applied to the low-Mw PMMA data presented in the previous section. The size of FVEs is known to vary substantially with Mw and temperature (41). The r_{0+1} radii using the p -hydrogen model were found to be 2.4 to 2.7 Å for the low-Mw PMMA oligomer at 260 K, which is a smaller average value and narrower distribution than found for the room-temperature high-Mw PMMA. Both effects can arise from better packing of the low-Mw PMMA oligomer due to its smaller size. Wobbling-in-a-cone and ROAM parameters for the low-Mw PMMA data can be found in *SI Appendix*.

Future studies of probe molecules with different shapes and without internal degrees of freedom will improve the parameterization of the probe dimensions. PhSeCN was used in this initial study because it has a very long lifetime, which permitted the second cone angle to be measured. However, rotation can occur around the C–Se bond between the SeCN and the phenyl ring. The barrier to this rotation is a small, 1.38 kcal/mol based on DFT studies of a single isolated molecule (*SI Appendix*). The rotation could either hinder or facilitate the reorientation of the molecule. In general, the center-of-mass motion of the probe molecule or possible strong intermolecular interactions between a probe and a polymer may also need to be taken into consideration.

The Vibrational Stark Effect and the Origin of the Inhomogeneous Line

The Onsager Reaction Field and Vibrational Solvatochromism. The nitrile stretch is known to exhibit vibrational solvatochromism (18, 42–44). In non-hydrogen-bonding systems, the transition frequency of the vibrational chromophore will shift based on the polarity of the solvating medium. This shift is very modest (usually on the order of a few wavenumbers) compared to that which is seen for electronic transitions. The origin of this solvatochromism in nitriles is ascribed to the first-order Stark effect coupling (18), that is, the vibrational transition frequency shift is proportional to the magnitude of the electric field projected along the dipole moment difference vector:

$$\omega = \omega_0 + \vec{F} \cdot \frac{\vec{\mu}}{\hbar}, \quad [6]$$

where ω is the vibrational transition frequency, μ is referred to as the Stark tuning parameter or dipole difference vector, and F is the electric field vector. The dipole difference vector is the difference in the permanent dipole in the vibrational ground and excited state. In nitriles, the dipole moment difference vector is coincident with both the transition dipole vector and the CN bond.

While the Stark coupling constant has been measured implicitly or explicitly for several nitriles (18, 44, 45), the coupling constant has not been measured for any R-selenocyanate. To determine the Stark tuning parameter, we have measured the central frequency of the nitrile transition of PhSeCN in 10 different nonaromatic solvents ranging from highly polar (dimethyl sulfoxide) to nonpolar (hexanes) using FTIR spectroscopy (Fig. 5A). The solvatochromatic shifts exhibited across the differing solvent environments can be related to the local electric field experienced by the probe molecule through the Onsager reaction field model (46). For a solute with permanent dipole μ_0 and index of refraction n embedded in a dielectric medium with dielectric constant ϵ , the field felt by the dipole goes as

$$\vec{F} = \frac{\vec{\mu}_0}{4\pi\epsilon_0 a^3} \left[\frac{2(\epsilon - 1)(n^2 + 2)}{3(2\epsilon + n^2)} \right], \quad [7]$$

where ϵ_0 is the permittivity of free space and a is the Onsager cavity radius, which depends on the molecular dimension.

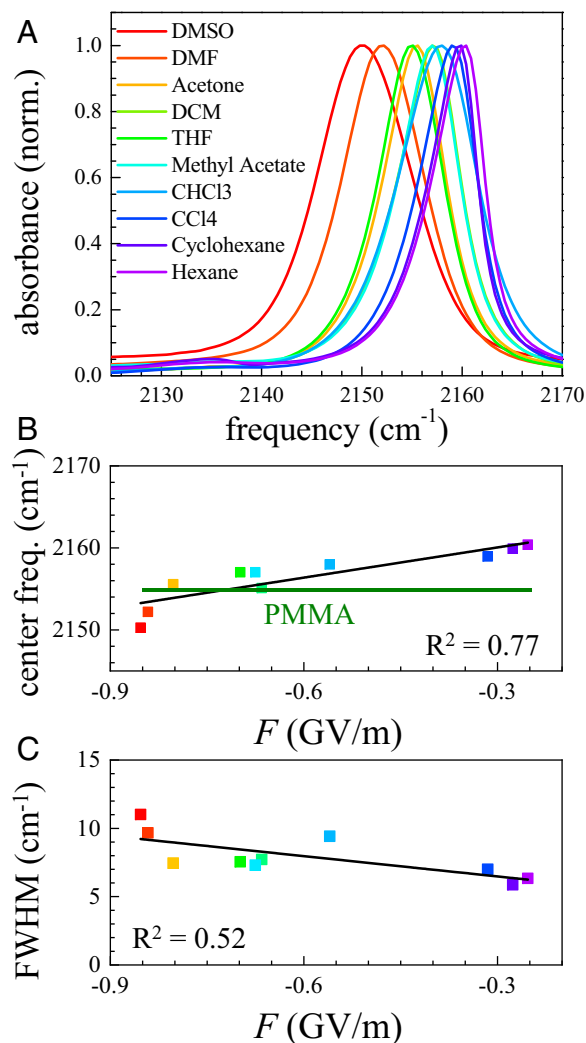


Fig. 5. Determining the vibrational Stark tuning rate for PhSeCN. (A) FTIR spectra of the CN stretch of PhSeCN in 10 common solvents of different polarity. Substantial vibrational solvatochromism is apparent. (B) Center frequencies of the PhSeCN absorptions relative to the Onsager reaction electric field calculated for each solvent (Eq. 7). Black line is a linear regression to determine the Stark tuning rate and the zero-field transition frequency. Green line indicates the center frequency of PhSeCN in PMMA. (C) FWHM of PhSeCN absorptions relative to the Onsager reaction field of each solvent. While the trend is noisier, it is apparent that the FWHM is correlated with the strength of the local electric fields.

Following the procedure of Boxer and coworkers (18), $a^3 = Mw/(\rho N_A)$, Mw is the Mw, ρ is the density, and N_A is Avogadro's number. For PhSeCN, $Mw = 182.1$ g/mol, $\rho = 1.484$ g/cm³, which gives $a^3 = 204$ Å³, $\mu_0 = 4$ D, and $n = 1.603$. By calculating the reaction field for each of the 10 solvent systems, the center frequency of the vibrational chromophore can be plotted against the reaction electric field F (Fig. 5B). Applying a linear regression, the values of the Stark tuning rate and the zero-field frequency were determined to be 12.3 ± 2.4 cm⁻¹/(GV/m) and $2,163.7 \pm 1.5$ cm⁻¹, respectively.

Performing the regression yields a fit that is comparable to those found for other aromatic nitriles and alkyl thiocyanates (18, 42). The deviations are systematic for each nitrile with the same solvent (18), indicating that the solvent-specific interactions [e.g., dipolar ordering (47) or dispersive and polarization effects (43)] are very similar for PhSeCN and the benzonitriles.

The Stark tuning rate of PhSeCN is high compared to benzonitrile, but it is within error of the range that was determined for substituted benzonitriles and alkyl thiocyanate compounds [5 to 12 cm⁻¹/(GV/m)]. Significantly, there was good agreement between the Stark tuning rates determined by the Onsager method and vibrational Stark spectroscopy of benzonitrile derivatives (18), so the determination for PhSeCN is reliable. A high Stark tuning rate is preferable for a vibrational chromophore, as it will be more sensitive to changes in the chemical environment.

The Stark effect can also be used to explain the extent of the inhomogeneous linewidth. An analogous trend can be seen in the FWHM's of the nitrile stretch against the Onsager reaction field (Fig. 5C). While still clear, this trend is much noisier than the center frequency trend due to the presence of motional narrowing. The ultrafast dynamics of the solvents cause the probe absorption line to have a narrower line shape, which only depends on the averaged field strength instead of the full inhomogeneous distribution of fields (48). The differing ultrafast dynamics for each solvent can cause the absorption peaks to be narrower than they would be otherwise.

The Stark effect analysis applied to PhSeCN in PMMA indicates that the center frequency of PhSeCN in PMMA corresponds to a ~ -0.7 GV/m electric field. Based on the vibrational Stark effect and the wobbling-in-a-cone model developed above, each frequency of the inhomogeneous line width of PhSeCN corresponds to both a local electric field and an average FVE size. This provides additional molecular level detail that is not accessible with other experimental techniques for studying FVEs. For the results presented here, a field of -1.1 GV/m is associated with a radius of 2.6 Å (short time cone of *p*-hydrogen model; Fig. 4B) on the red side of the spectrum and a field of -0.3 GV/m with a radius of 3.2 Å on the blue side. This assignment was also successfully applied to the 1-to-2 transition (SI Appendix).

While the Onsager model is useful and has been shown to be consistent with the results of vibrational Stark spectroscopy (18), the limits of the model should also be considered. The Onsager model uses a dielectric continuum and predicts a uniform reaction field, while actual field strengths on the atomic scale can be highly heterogeneous and rapidly varying. The calculated field strength also reflects the projection of the field onto the CN dipole rather than an absolute magnitude. Some of the observed solvatochromism may also arise from non-Stark-effect interactions (43).

These details provide a simple heuristic picture of the frequency-dependent anisotropy's behavior. The red side of the absorption spectrum corresponds to probe molecules that are in small FVEs, close to the polar polymer backbone, giving both a large effective field and a high degree of confinement. The blue side of the band, by contrast, has probe molecules that are less confined in larger FVEs which are on average farther from the polymer backbone.

The Effect of the Local Electric Fields on the Pump-Probe Experiments.

In addition to shifting the vibrational frequency through the Stark effect, the presence of a strong local field can also cause some degree of orientational ordering of a static dipole as determined by a Boltzmann distribution. Although the sample is macroscopically isotropic, such ordering will result in a locally nonisotropic orientational distribution in a similar manner as the hard cone of the wobbling-in-a-cone model. The field-induced ordering can be related to an order parameter analogous to that in Eq. 5 by (49)

$$S = \langle P_2(\cos\theta) \rangle = \frac{3 + x^2 - 3x \coth(x)}{x^2}, \quad x = \frac{\mu_0 F}{kT}, \quad [8]$$

where T is the absolute temperature, k is the Boltzmann constant, μ_0 is the magnitude of the permanent dipole of the probe molecule, and F is the magnitude of the local electric field. For room temperature at the average magnitude of the field experienced by a probe molecule ($F = -0.7$ GV/m, $\mu_0 = 4$ D), we find

that the order parameter for the orientation of the PhSeCN molecules would be $S = 0.229$, which corresponds to a hard cone of angle of 70° by Eq. 5. This is much larger than the largest cone given by the wobbling-in-a-cone model used in analyzing the pump-probe data (27.5° for the center frequency). The electric field would have to be a massive -5.3 GV/m to produce the observed ordering for the center frequency at room temperature. Similarly, a formula for a combined order parameter with both an electric field and hard cone was determined (SI Appendix). Using the field strengths determined from the Stark effect analysis, the cone angles determined from the experimental order parameters (Fig. 2B) have a negligible contribution from the electric field ordering.

Despite the lack of electric field-induced ordering as determined from the second-order Legendre polynomial order parameter (Eq. 8), there is still some alignment of the probe molecules' dipoles along the local electric field. The order parameter that determines if the dipoles are aligned with the electric field (and that the measured electric field is always negative) is the first Legendre polynomial order parameter, $\langle \cos\theta \rangle$. The parameter is determined as (49)

$$\langle \cos\theta \rangle = \frac{\int_0^{2\pi} d\phi \int_0^\pi d\theta \sin(\theta) \exp(x \cos\theta) \cos\theta}{\int_0^{2\pi} d\phi \int_0^\pi d\theta \sin(\theta) \exp(x \cos\theta)}, \quad x = \frac{\mu_0 F}{kT} \quad [9]$$

$$\langle \cos\theta \rangle = \coth(x) - \frac{1}{x}.$$

The first Legendre order parameter will always be larger than the second Legendre order parameter (Fig. 6). Using the calculated electric field strengths from the solvatochromism of PhSeCN, the values of $\langle \cos\theta \rangle$ range from 0.4 to 0.7, indicating moderate to high ordering under the field. This result shows that we would simultaneously expect to see only a negative projection of the electric field onto the probe difference dipole and minimal impact on the pump-probe experiment's observables.

These results show that the PhSeCN probe molecule is experiencing substantial steric confinement that is independent of ordering by the local electric fields. As the inertial and first diffusive cones are even smaller, the extent of confinement and radii of the FVEs are related to the sizes of the nanoscopic domains in the polymer rather than the local electric fields.

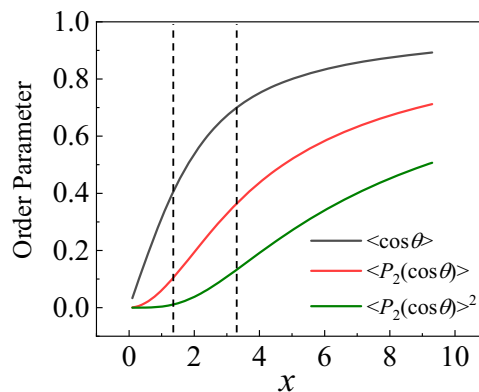


Fig. 6. Calculations for the orientational order parameters as a function of electric field strength (proportional to x). For the local field strengths measured using the solvatochromism of PhSeCN (dashed lines), there is substantial ordering in $\langle \cos\theta \rangle$ (Eq. 9), but much less ordering in $\langle P_2(\cos\theta) \rangle$ (Eq. 8). The pump-probe order parameter is $\langle P_2(\cos\theta) \rangle^2$. This result shows that the probe molecule dipoles tend to align to the local electric field, but the order parameter measured by the pump-probe experiment will be largely unaffected.

Concluding Remarks

Ultrafast IR polarization-selective pump-probe ROAM is a useful technique for determining FVE sizes and distributions in glassy polymers as well as fast polymer structural dynamics and local electric fields. The solvatochromatic properties of vibrational probes cause them to absorb IR light at different vibrational frequencies when located in distinct polymer environments. The orientational relaxation dynamics of the probe molecules were found to be highly dependent on that vibrational frequency. At all frequencies, only partial orientational relaxation was observed, demonstrating that the probe molecules are in highly confined environments. Companion experiments on a low-Mw PMMA oligomer showed that the observed frequency dependence is a property of the glassy state in which the macroscopic structural evolution is exceedingly slow.

By measuring the highly constrained dynamics of the PhSeCN probe molecule and using the wobbling-in-a-cone model and the molecular dimensions of PhSeCN, we were able to determine FVE sizes. As there are two distinct timescales in the orientational relaxation, two separate FVE size distributions were extracted. The fast timescale was associated with the instantaneous distribution of free volumes. The slow timescale cone dynamics were associated with larger volumes. The larger radii at longer time, which are a result of local structural fluctuations of the polymer, reflect all accessible volume, but all of this larger volume is not simultaneously available. The long time dynamics that result in the larger cone angles are the result of shape fluctuations of the FVEs that leave the ensemble average volumes unchanged. The instantaneous distribution of PMMA FVE radii determined with ROAM agrees well with measurements made with PALS, the best method in the literature for measuring FVE dimensions.

The solvatochromism of the vibrational probe, a key feature of the experiments, was explained by the vibrational Stark effect. The Stark coupling parameter for PhSeCN was determined by measuring the CN stretch vibrational spectrum in 10 solvents and using the standard Onsager reaction field method, which has been previously applied to other nitriles (18, 42). The measured local electric fields are not strong enough to influence the pump-probe experimental cone angle determination, but strong enough to induce some alignment of the probe dipoles along the electric field. Using the Stark coupling parameter, a local electric field was associated with each FVE size, with the strongest fields corresponding to the smallest volume elements.

ROAM should be applicable to a wide range of polymeric solids. The experiments presented here extracted a great deal of information using a single vibrational probe. There is the possibility of extracting more information using ROAM by varying the vibrational probe. By changing the size, shape, and chemical behavior of the embedded probe molecule, a more expansive molecular level description of FVEs and their dynamics can emerge.

Data Availability. All relevant data are included in the paper and *SI Appendix*.

ACKNOWLEDGMENTS. This work was supported by Office of Naval Research Grant N00014-17-1-2656. We thank J. E. Thomaz for helpful discussions and feedback; Prof. Binny Cherayil (IISc) for helpful discussions on the P5PP observable; and J. Nishida, R. Yuan, S. A. Yamada, J. P. Breen, and B. Wu for help constructing the ultrafast IR equipment. We also thank Prof. Gregory Sotzing's group at the University of Connecticut for useful discussion regarding sample preparation. We thank our reviewers for constructive feedback that improved this manuscript.

- R. P. White, J. E. G. Lipson, Polymer free volume and its connection to the glass transition. *Macromolecules* **49**, 3987–4007 (2016).
- D. Turnbull, M. H. Cohen, Free-volume model of the amorphous phase: Glass transition. *J. Chem. Phys.* **34**, 120–125 (1961).
- M. H. Cohen, D. Turnbull, Molecular transport in liquids and glasses. *J. Chem. Phys.* **31**, 1164 (1959).
- Z. X. Low, P. M. Budd, N. B. McKeown, D. A. Patterson, Gas permeation properties, physical aging, and its mitigation in high free volume glassy polymers. *Chem. Rev.* **118**, 5871–5911 (2018).
- T. S. Chow, Kinetics of free volume and physical aging in polymer glasses. *Macromolecules* **17**, 2336–2340 (1984).
- R. E. Robertson, Segmental mobility in the equilibrium liquid below the glass transition. *Macromolecules* **18**, 953–958 (1985).
- W. G. Knauss, I. J. Emri, "Non-linear viscoelasticity based on free volume consideration" in *Computational Methods in Nonlinear Structural and Solid Mechanics*, H. G. McComb, Ed. (Pergamon Press Ltd, 1981), pp. 123–128.
- J. C. Bauwens, Attempt to correlate the formation of free volume and the plastic deformation process in glassy polymers. *Polymer* **21**, 699–705 (1980).
- R. Greiner, F. R. Schwarzl, Thermal contraction and volume relaxation of amorphous polymers. *Rheol. Acta* **23**, 378–395 (1984).
- J. Artbauer, Electric strength of polymers. *J. Phys. D Appl. Phys.* **29**, 446–456 (1996).
- J. C. Jansen *et al.*, Comparative study of different probing techniques for the analysis of the free volume distribution in amorphous glassy perfluoropolymers. *Macromolecules* **42**, 7589–7604 (2009).
- Y. P. Yampolskii, Methods for investigation of the free volume in polymers. *Russ. Chem. Rev.* **76**, 59–78 (2007).
- H.-S. Tan, I. R. Piletic, M. D. Fayer, Polarization selective spectroscopy experiments: Methodology and pitfalls. *J. Opt. Soc. Am. B* **22**, 2009 (2005).
- A. Tokmakoff, Orientational correlation functions and polarization selectivity for nonlinear spectroscopy of isotropic media. 1. Third order. *J. Chem. Phys.* **105**, 1–12 (1996).
- Y. L. A. Rezus, H. J. Bakker, On the orientational relaxation of HDO in liquid water. *J. Chem. Phys.* **123**, 114502 (2005).
- M. Cho, G. R. Fleming, S. Mukamel, Nonlinear response functions for birefringence and dichroism measurements in condensed phases. *J. Chem. Phys.* **98**, 5314 (1993).
- S. Mukamel, *Principles of Nonlinear Optical Spectroscopy*, (Oxford University Press, New York, 1995).
- N. M. Levinson, S. D. Fried, S. G. Boxer, Solvent-induced infrared frequency shifts in aromatic nitriles are quantitatively described by the vibrational Stark effect. *J. Phys. Chem. B* **116**, 10470–10476 (2012).
- C. Wästlund, F. H. J. Maurer, Positron lifetime distributions and free volume parameters of PEO/PMMA blends determined with the maximum entropy method. *Macromolecules* **30**, 5870–5876 (1997).
- S. K. Karthick Kumar, A. Tamimi, M. D. Fayer, Comparisons of 2D IR measured spectral diffusion in rotating frames using pulse shaping and in the stationary frame using the standard method. *J. Chem. Phys.* **137**, 184201 (2012).
- C. Yan *et al.*, Ultrafast to ultraslow dynamics of a Langmuir monolayer at the air/water interface observed with reflection enhanced 2D IR spectroscopy. *J. Am. Chem. Soc.* **139**, 16518–16527 (2017).
- D. J. Hoffman, K. P. Sokolowsky, M. D. Fayer, Direct observation of dynamic crossover in fragile molecular glass formers with 2D IR vibrational echo spectroscopy. *J. Chem. Phys.* **146**, 124505 (2017).
- D. E. Moilanen *et al.*, Water inertial reorientation: Hydrogen bond strength and the angular potential. *Proc. Natl. Acad. Sci. U.S.A.* **105**, 5295–5300 (2008).
- H. S. Tan, I. R. Piletic, M. D. Fayer, Orientational dynamics of water confined on a nanometer length scale in reverse micelles. *J. Chem. Phys.* **122**, 174501 (2005).
- G. Lipari, A. Szabo, Model-free approach to the interpretation of nuclear magnetic resonance relaxation in macromolecules. 1. Theory and range of validity. *J. Am. Chem. Soc.* **104**, 4546–4559 (1982).
- G. Lipari, A. Szabo, Effect of librational motion on fluorescence depolarization and nuclear magnetic resonance relaxation in macromolecules and membranes. *Biophys. J.* **30**, 489–506 (1980).
- P. L. Kramer, C. H. Giammanco, M. D. Fayer, Dynamics of water, methanol, and ethanol in a room temperature ionic liquid. *J. Chem. Phys.* **142**, 212408 (2015).
- J. G. Victor, J. M. Torkelson, On measuring the distribution of local free volume in glassy polymers by photochromic and fluorescence techniques. *Macromolecules* **20**, 2241–2250 (1987).
- D. J. Hoffman, M. D. Fayer, Discontinuity in fast dynamics at the glass transition of ortho-terphenyl. *J. Phys. Chem. B* **121**, 10417–10428 (2017).
- T. G. Fox, P. J. Flory, The glass temperature and related properties of polystyrene. Influence of molecular weight. *J. Polym. Sci., Polym. Phys. Ed.* **14**, 315–319 (1954).
- K. M. O'Connor, K. M. Scholsky, Free volume effects on the melt viscosity of low molecular weight poly(methyl methacrylate). *Polymer* **30**, 461–466 (1989).
- Y. H. Zhao, M. H. Abraham, A. M. Zissimos, Fast calculation of van der Waals volume as a sum of atomic and bond contributions and its application to drug compounds. *J. Org. Chem.* **68**, 7368–7373 (2003).
- L. David *et al.*, Density fluctuations in amorphous systems: SAXS and PALS results. *J. Non-Cryst. Solids* **235–237**, 383–387 (1998).
- C. L. Wang, T. Hirade, F. H. J. Maurer, M. Eldrup, N. J. Pedersen, Free-volume distribution and positronium formation in amorphous polymers: Temperature and positron-irradiation-time dependence. *J. Chem. Phys.* **108**, 4654–4661 (1998).

35. R. J. Elwell, R. A. Pethrick, Positron annihilation studies of poly(methyl methacrylate) plasticized with dicyclohexyl phthalate. *Eur. Polym. J.* **26**, 853–856 (1990).
36. J. S. Royal, J. G. Victor, J. M. Torkelson, Photochromic and fluorescent probe studies in glassy polymer matrices. 4. Effects of physical aging on poly(methyl methacrylate) as sensed by a size distribution of photochromic probes. *Macromolecules* **25**, 729–734 (1992).
37. S. J. Tao, Positronium annihilation in molecular substances. *J. Chem. Phys.* **56**, 5499–5510 (1972).
38. M. Eldrup, D. Lightbody, J. N. Sherwood, The temperature dependence of positron lifetimes in solid pivalic acid. *Chem. Phys.* **63**, 51–58 (1981).
39. R. Bergman, F. Alvarez, A. Alegria, J. Colmenero, Dielectric relaxation in PMMA revisited. *J. Non-Cryst. Solids* **235–237**, 580–583 (1998).
40. P. A. O'Rourke Muisener *et al.*, Effects of gamma radiation on poly(methyl methacrylate)/single-wall nanotube composites. *J. Mater. Res.* **17**, 2507–2513 (2002).
41. Z. Yu, U. Yahsi, J. D. McGervey, A. M. Jamieson, R. Simha, Molecular weight-dependence of free volume in polystyrene studied by positron annihilation measurements. *J. Polym. Sci., B, Polym. Phys.* **32**, 2637–2644 (1994).
42. L. J. G. W. van Wilderen, D. Kern-Michler, H. M. Müller-Werkmeister, J. Bredenbeck, Vibrational dynamics and solvatochromism of the label SCN in various solvents and hemoglobin by time dependent IR and 2D-IR spectroscopy. *Phys. Chem. Chem. Phys.* **16**, 19643–19653 (2014).
43. B. Błasiak, A. W. Ritchie, L. J. Webb, M. Cho, Vibrational solvatochromism of nitrile infrared probes: Beyond the vibrational Stark dipole approach. *Phys. Chem. Chem. Phys.* **18**, 18094–18111 (2016).
44. S. Bagchi, S. D. Fried, S. G. Boxer, A solvatochromic model calibrates nitriles' vibrational frequencies to electrostatic fields. *J. Am. Chem. Soc.* **134**, 10373–10376 (2012).
45. S. S. Andrews, S. G. Boxer, Vibrational Stark effects of nitriles II. Physical origins of Stark effects from experiment and perturbation models. *J. Phys. Chem. A* **106**, 469–477 (2002).
46. L. Onsager, Electric moments of molecules in liquids. *J. Am. Chem. Soc.* **58**, 1486–1493 (1936).
47. J. G. Kirkwood, The dielectric polarizability of polar liquids. *J. Chem. Phys.* **7**, 911–919 (1937).
48. P. Hamm, M. Zanni, *Concepts and Methods of 2D Infrared Spectroscopy*, (Cambridge University Press, 2011).
49. S. Stallinga, Effect of rotational diffusion in an orientational potential well on the point spread function of electric dipole emitters. *J. Opt. Soc. Am. A Opt. Image Sci. Vis.* **32**, 213–223 (2015).